Editors' Suggestion

Fracture initiation in silicate glasses via a universal shear localization mechanism

Matthieu Bourguignon,[1] Gustavo Alberto Rosales-Sosa,[2] Yoshinari Kato,[2] Bruno Bresson,[1] Hikaru Ikeda,[2] Shingo Nakane,[2] Gergely Molnár,[3] Hiroki Yamazaki,[2] and Etienne Barthel[1]

[1]*Soft Matter Sciences and Engineering, ESPCI Paris, PSL University, CNRS, Sorbonne University, 75005 Paris, France*

[2]*Nippon Electric Glass, 7-1, Seiran 2-Chome, Otsu, 520-8639 Shiga, Japan*

[3]*CNRS, INSA Lyon, LaMCoS, UMR5259, 69621 Villeurbanne, France*

(Received 23 January 2026; accepted 23 March 2026; published 8 June 2026)

Shear bands lie at the root of fracture initiation in bulk metallic glasses and amorphous polymers. For silicate glasses, in contrast, studies have largely emphasized permanent volumetric strain, commonly referred to as densification. Here, we systematically investigate indentation-induced fracture in two distinct families of aluminoborosilicate glasses. The results demonstrate that plastic shear flow plays a decisive role in governing fracture initiation. In addition, molecular dynamics simulations reveal a pronounced composition dependence of softening associated with plastic shear flow, closely mirroring the experimentally observed propensity for strain localization. We conclude that silicate glasses conform to a universal pattern of rupture initiation governed by the localization of shear-deformation, aligning with a broad range of amorphous materials, including bulk metallic glasses and glassy polymers.

DOI: 10.1103/l936-nk13

I. INTRODUCTION

Despite decades of intensive research, a comprehensive understanding of the rupture properties of silicate glasses remains a significant challenge [1], constraining mitigation strategies. A range of conceptual frameworks has been advanced, including the tailoring of network connectivity [2], the notion of optimal topological rigidity [3] (often illustrated by highly connected networks such as silicon oxynitrides or carbides [4]), or, from a quite different perspective, the ideas of nanoscale ductility [3] or adaptive network structures [5]. These approaches, however, offer limited predictive capability and have yet to establish clear, quantitative relationships between glass composition, underlying deformation mechanisms, and macroscopic mechanical performance.

One of the difficulties is that, in very practical terms, the fracture sensitivity of silicate glasses is usually probed by indention, indeed a technique of choice for characterizing the nonlinear deformation, damage, and fracture processes in brittle materials [6]. In particular, indentation cracking provides a convenient and quantitative measure of crack resistance (CR), the resistance to indentation-induced damage [7,8]. In fact, although CR, defined as the threshold load required to initiate median or radial cracks beneath a Vickers indenter tip, may seem somewhat primitive at first glance, it has proven to be highly discriminating for silicate glasses [9].

The strain field under the tip is complex, but extensive studies over more than half a century [10–13] have provided a robust foundation for a general understanding of the ensuing damage and fracture processes. Silicate glasses, however, undergo irreversible volumetric deformation, or densification [14], which reduces indentation-induced stresses and can therefore partially suppress crack initiation and propagation [15,16]. As a result, over the past decades, considerable effort has been devoted to quantifying the role of densification in decreasing the cracking sensitivity of silicate glasses [17,18]. Notably, low atomic packing density and a low Poisson's ratio, both linked to enhanced densification, have been reported to correlate with improved crack resistance [4,19].

In contrast to this densification-oriented perspective, an alternative framework was developed in the 1980s, highlighting localized shear deformation as the primary mechanism governing fracture initiation. Experimental studies showed that cracks often originate at discrete shear events, referred to as shear faults or slip events, which appear during loading and serve as deformation-induced crack nuclei [20–22]. This line of investigation, however, has received comparatively little attention in recent years, with only one notable exception [23].

To clarify the relative contributions of the different mechanisms proposed for fracture initiation in silicate glasses in relation to their composition and structure, we conducted a systematic investigation of indentation cracking across two families of glass compositions spanning a broad range of crack resistances. One of these families comprises Ca alumino-boro-silicate glasses: the influence of silicon substitution by boron on crack resistance is well established and has been extensively studied [24], although a complete understanding of the mechanisms underlying boron-induced strengthening remains elusive. To broaden the scope of our conclusions, we also examined the effect of network modifier field strength, substituting Mg for Ca, another well-known strategy for drastically improving crack resistance [25,26].

Within these compositional ranges, we find compelling evidence that crack resistance correlates strongly with the morphology of shear bands, while exhibiting no significant dependence on Poisson's ratio or on the densification behavior. This finding demonstrates that, in silicate glasses, the intrinsic resistance to localized shear faulting controls the macroscopic cracking response under sharp-contact

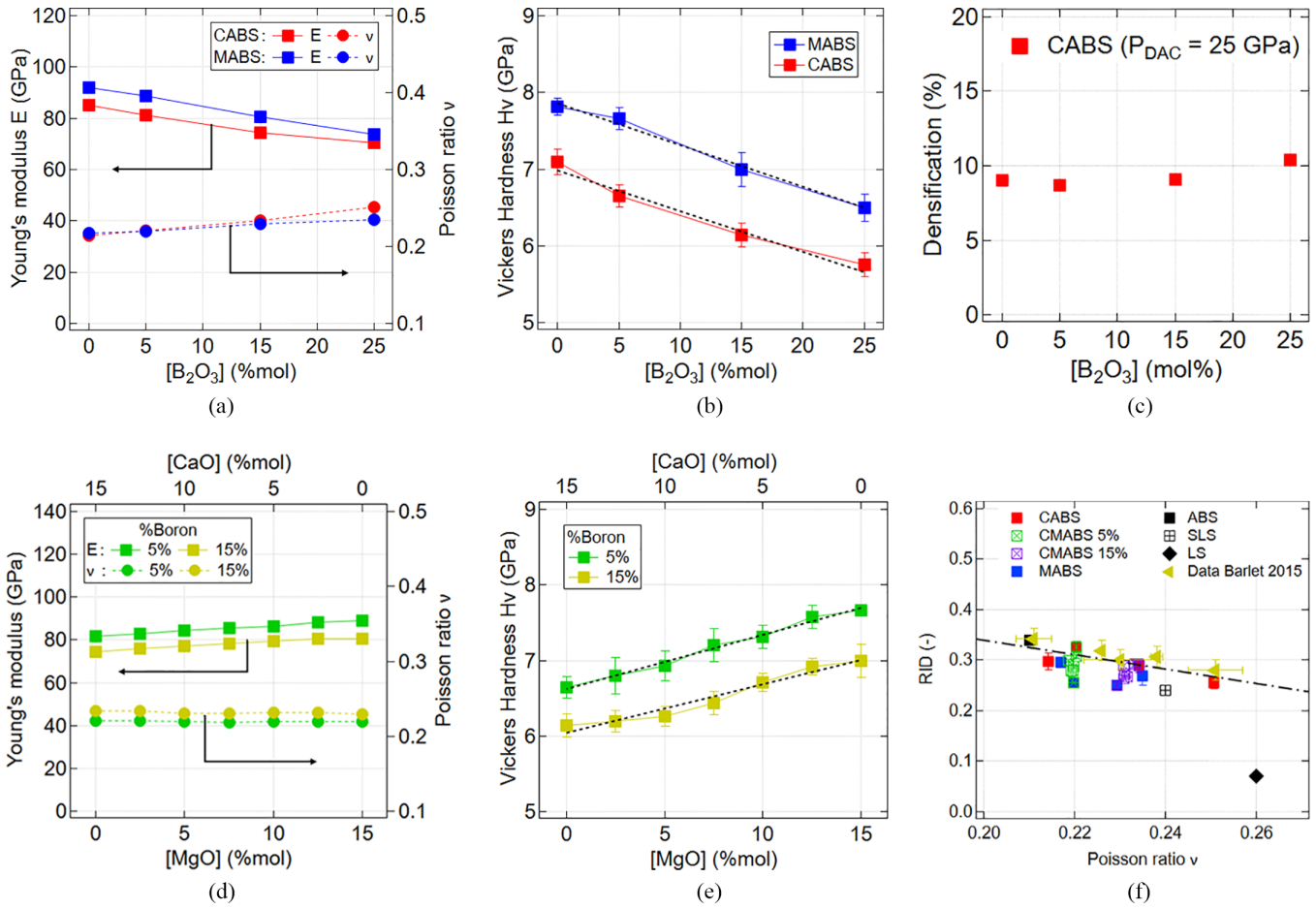

FIG. 1. (a)–(c) single alkaline earth (Ca or Mg) ABS glasses with varying B_2O_3 content: (a) Young's Modulus E and Poisson's ratio ν; (b) micro-indentation Vickers hardness H_V; (c) densification (CABS only) at 25 GPa (multianvil cell) [28]; (d)–(e) mixed alkaline earth ABS glasses (5% or 15% B_2O_3) as a function of Mg vs Ca content: (d) Young's Modulus E and Poisson ratio ν; e) micro-indentation Vickers hardness H_V; (f) all glass compositions: RID as a function of Poisson ratio including some (LS, SLS, ABS) glasses from Kato *et al.* [29] and from Barlet *et al.* [18]. Error bars are not shown if smaller than the marker size.

loading. Shear flow and the associated material instabilities thus emerge as a unifying paradigm of fracture behavior in amorphous materials, one that silicate glasses, despite their capacity for densification, share with, *e.g.,* metallic glasses and glassy polymers.

II. RESULTS

Eighteen glass samples were melted (see [27] Sec. I) with the nominal composition $(15-y)\mathrm{CaO}\cdot y\mathrm{MgO}\cdot 15\mathrm{Al_2O_3}\cdot x\mathrm{B_2O_3}\cdot(70-x)\mathrm{SiO_2}$ (CMABS glasses). The boron content (x) was varied as 0, 5, 15, and 25 mol% (Table S1 [27]). For compositions with $x = 5$ and 15 mol%, CaO was progressively substituted by MgO, with $y = 0$ (CABS), 2.5, 5, 7.5, 10, 12.5, and 15 (MABS) mol% (Table S2). In addition, reference glasses previously reported by Kato *et al.* [24] were also prepared for comparison.

A. General mechanical properties

Key mechanical properties were systematically characterized and are presented in Fig. 1, with numerical values provided in Supplemental Material, Sec. SI [27]. Young's modulus E and shear modulus G were measured with the resonance method and hardness H with microindentation under a load of 100 gf.

Overall, the property evolutions were moderate across the present compositional changes. Incorporating 25 mol% B_2O_3 led to a 20% reduction in both Young's modulus and hardness. Conversely, substituting Mg^{2+} for Ca^{2+} resulted in a marginal 5% increase in E and a 10% increase in H. Regarding Poisson's ratio, the 25 mol% B_2O_3 addition caused a 20% increase in the CABS system and a 10% increase for the MABS system, while the Mg^{2+} for Ca^{2+} substitution had a negligible effect on ν.

The ability of the glasses to densify was also investigated. For the CABS series, densification under hydrostatic pressure was measured up to 25 GPa using a multianvil cell (MAC) [28]. As is common with borosilicates, an intermediate value of the densification at saturation of approximately 10% was observed. There is no measurable dependence of this value on boron content [Fig. 1(c)]. Due to the difficulties associated with MAC measurements, another quantity is often used as an approximate quantification of densification, the recovery of indentation depth (RID) method [9,26,30]. This method relies on the understanding that the recovery of

indentation depth observed upon annealing an indent close to T_g is predominantly due to density recovery, and not to shear flow recovery. In contrast to the MAC measurements, it is not a direct measurement of densification, but is often used for a simple, approximate evaluation. Vickers indentation depths, d_{before} and d_{after}, were measured before and after annealing at 0.9 T_g for 2 h, and the RID was calculated as

$$\text{RID} = \frac{d_{\text{before}} - d_{\text{after}}}{d_{\text{before}}}. \quad (1)$$

The measured RID values are approximately 0.3 and exhibit minimal variation across the compositions studied in this work [Fig. 1(f)]. A correlation with Poisson's ratio is observed, characterized by a slight decrease in RID with increasing Poisson's ratio, consistent with previous observations [31]. Overall, these results agree well with those reported by Barlet *et al.* [18] for glasses of similar compositions.

B. Crack resistance

To determine the crack resistance (CR), the pristine glass samples were indented using a Vickers indenter under controlled environmental conditions (25 °C and 30% relative humidity). Radial crack formation at the indentation corners was systematically recorded. The applied load was incrementally increased from 100 gf to 6 kgf, with 40 indentations performed at each load. The probability of crack initiation P_{CI} was calculated as the total number of observed radial cracks n_{RC} over 4, the total number of indentation corners. The crack resistance, CR, was defined as the applied load corresponding to $P_{\text{CI}} = 50\%$.

The measured CR values for all compositions are plotted in Fig. 2. In contrast to the other mechanical properties, CR exhibited a strong compositional dependence. For the CABS series [Fig. 2(a)], increasing the B_2O_3 content from 0 to 25 mol% resulted in a significant ten-fold increase in CR. Similarly, when the B_2O_3 content was fixed at 5 mol% [Fig. 2(b)], substituting MgO for CaO initially caused a slight decrease in CR between 0 and 5 mol% MgO, followed by a substantial three-fold increase between 5 mol% and 15 mol% MgO. However, at the maximum B_2O_3 content of 25 mol%, the CR remained high (approximately 30 N) and was virtually unaffected by the MgO for CaO substitution. This insensitivity was mirrored when B_2O_3 content was varied in the presence of 15 mol% MgO. Collectively, these results strongly suggest that the strengthening mechanisms induced by the addition of boron and the addition of magnesium represent two distinct and independent effects.

The CR is plotted as a function of RID in Fig. 2(c). As expected from the weak variation of RID and the large variation of CR across the composition range, we observe only a very weak dependence of CR on RID, in contrast to previous reports [4,32]. Interestingly, the slope of this dependence is negative, which is unexpected in the light of presently accepted trends. For completeness, data for the same commercial glass compositions (LS, SLS, and ABS) investigated by [9] have been added to the plot (black markers). For these three glasses, a clear positive correlation between CR and RID is observed, conforming to the accepted ideas. These opposing trends are summarized in Fig. 2(d), where arrows indicate the direction of change in crack resistance. These observations reinforce the view that the correlation between CR and RID postulated, e.g., in Ref. [17] is only partial, as previously noted [2].

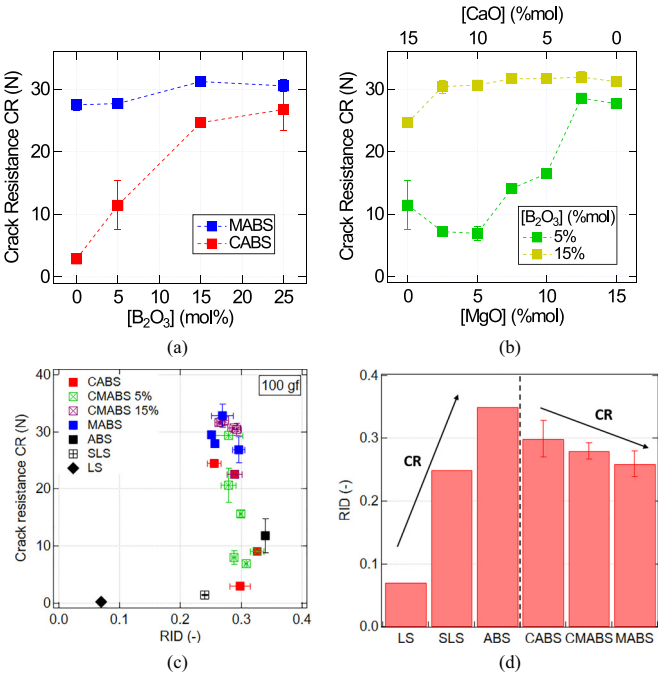

FIG. 2. (a) and (b) Crack resistance CR of (a) single alkaline earth network modifier ABS glasses and (b) mixed alkaline earth network modifiers ABS glasses. If no error bar is shown, it is less than the marker's size. (c) Crack resistance (CR) as a function of recovered indentation depth (RID) and (d) recovered indentation depth for different silicate glasses compositions, including some (LS, SLS, ABS) from Kato *et al.* [29]. Arrows show how crack resistance increases with compositions.

C. Indentation cross sections and shear bands

Plastic flow under indentation was investigated as a function of glass composition using the bonded interface technique [23,33]: indentation over a pre-existing crack near the crack tip, followed by full crack opening, provided cross sections of 1 kgf indents for a wide range of compositions.

Figure 3 presents the results for both series of compositions, revealing a gradual evolution in the cross-section morphologies. The CAS glass (boron- and magnesium-free) exhibits pronounced shear localization, manifested as a fairly regular network of darker lines within the plastic zone. As B_2O_3 gradually substitutes for SiO_2 (from top to bottom), these shear faults progressively disappear and are replaced by a homogeneous area with a lighter grey shade. This transformation first appears in the central part of the plastic zone and subsequently extends towards the edges. A similar transition is observed when Mg^{2+} is substituted for Ca^{2+} (from left to right). In the high boron, high magnesium composition, the plastic zone, which is easily discernible by its lighter gray shade, appears completely homogeneous. Remarkably, this evolution closely parallels the progressive increase of the crack resistance reported in the previous section, from

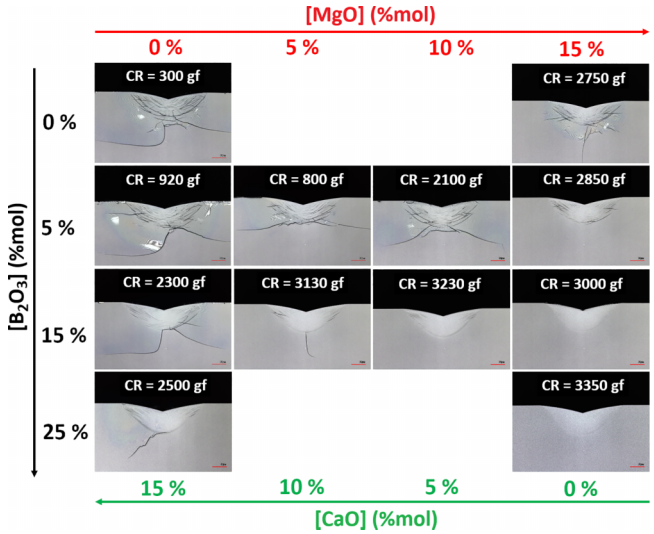

FIG. 3. Sum up of all cross sections through 1 kgf Vickers indents.

approximately 300 gf for CAS to 3350 gf for the 25 mol% B_2O_3 and 15 mol% Mg^{2+} compositions.

Figure 4 displays cross sections at 1 kgf for four mixed network modifier compositions, providing a clearer visualization of the distribution of shear faulting within the plastic zone. In the magnesium-free composition with 5 mol% B_2O_3 (CABS2), shear faults are observed across the entire plastic zone, exhibiting the concentric distribution of shear bands under indentation and the symmetric sets of secondary 'spiral' bands characteristic of normal silicate glasses [33] or BMGs [34]. This composition exhibits a low CR of approximately 900 gf, and both median and lateral cracks are visible. Upon the addition of 10 mol% MgO (CMABS4), the CR doubles, and the central part of the deformation zone contains fewer visible shear faults, while the edges show similar shear patterns to the CABS2 composition. A similar trend is observed for the CABS glass with 15 mol% B_2O_3 (CABS3), where the central part of the indent is shear-fault free, yet the edges of the deformation zone still display a high density of shear bands/faults. Finally, with the addition of both boron and magnesium (CMABS9), the central part of the plastic zone becomes smoother, minimal shear localization is discernible

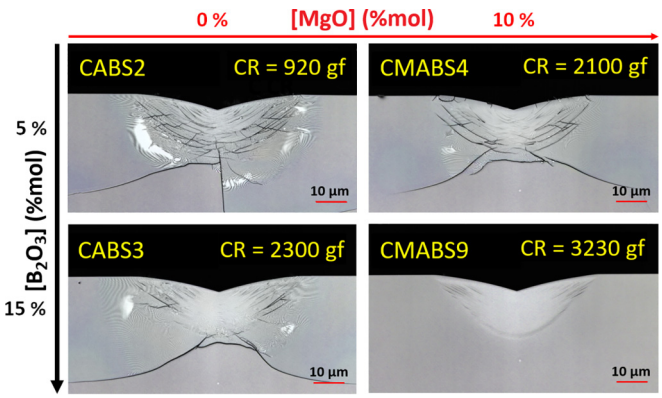

FIG. 4. Cross sections through 1 kgf Vickers indents in (a) CABS2, (b) CMABS4, (c) CABS3, and (d) CMABS9.

on the edges, and the lateral crack has disappeared. In this glass, the CR exceeds 3000 gf.

Finally, the commercial compositions studied in [9] have also been investigated, and their cross-sectional views for 1 kgf indents are provided in Supplemental Material ([27] Fig. S3) along with their CR taken from [9], confirming that the correlation between CR and shear banding also holds for these compositions.

These observations extend the work of Gross *et al.* [23] by demonstrating that CR systematically increases as shear faults become less pronounced, a behavior observed across all compositions studied.

D. Roughness measurements of the plastically deformed region

In the bonded interface method, shear bands intersect the original crack faces as slip steps [35] [Figs. 5(a) and (zoom) 5(b)]. As a result, in our experiments, the characteristics of the shear bands affect the corrugation of the cross section. To quantify shear band activity under loading, we measured the surface roughness of the cross section using standard topography parameters: roughness amplitude R_a and characteristic lateral size RS_m. These measurements were performed on the central region beneath the indenter using laser scanning microscopy. Multi-lines used to measure roughness were drawn vertically onto the center of the deformation zone where shear bands intersect each other horizontally.

Figure 5(c) illustrates the relationship between CR and the mean roughness R_a, measured from cross sections of 1 kgf Vickers indents. This correlation indicates that more crack-resistant glasses, such as the high-boron compositions, exhibit lower roughness over the center of the plastic zone, suggesting less pronounced shear localization. Conversely, compositions with low crack resistance display higher roughness, i.e., more significant shear bands, as exemplified by the lead silicate glass.

We also investigated the effect of indentation load. Since shear bands initiate on the edge of the plastic zone, by geometrical invariance, a shear band that initiates under higher load develops a larger slip [34]. Consequently, we find a larger surface roughness at the bottom of the plastic zone for a 1 kgf indent than for 500 gf [Fig. 5(d)]. The ratio of approximately 1.2 in R_a between the two loads is consistent with the $\sqrt{2}$ scaling expected from the self-similarity of the indentation process.

Finally, we have also calculated the characteristic correlation distance RS_m in the roughness profiles, which is expected to reflect the spacing between shear bands. Stronger shear bands associate with larger slip and increased spacing, resulting in a decrease of crack resistance with RS_m [Fig. 5(e)].

E. Structural rearrangements and shear deformation mechanisms

To corroborate these macroscopic observations and relate them to the intrinsic structural features of the glass, we employed molecular dynamics (MD)–or more precisely molecular statics–simulations. MD is a well-established tool for probing the mechanical response of model amorphous materials.

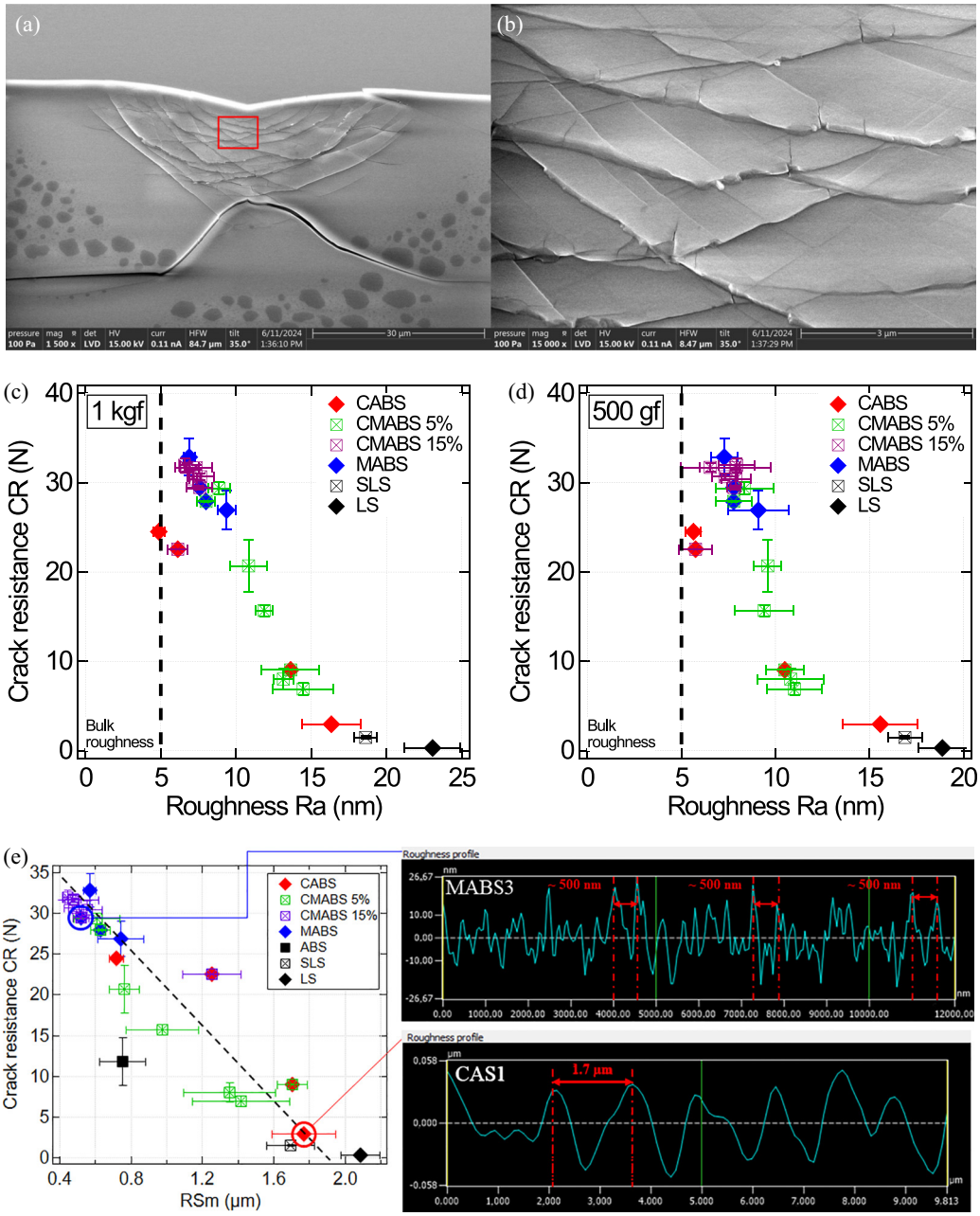

FIG. 5. (a) Scanning electron image of 1kgf Vickers indentation cross section in soda-lime silicate glass and (b) magnified image of shear bands from the cross section. The sample has been tilted to 35° to observe shear bands from the bottom. (c) and (d) Relationship between crack resistance (CR) and roughness (R_a) for Vickers indentation cross sections at 1 kgf (c) and 500 gf (d), including some commercial compositions (black markers) from Kato *et al.* [9]. The vertical dashed line is determined as the bulk roughness. (e) Crack resistance as a function of the average spacing RS_m between shear bands from Vickers indentation cross sections at 1 kgf for all glass compositions. Data are available at [36].

For generic amorphous systems, MD studies have shown that shear localization initiates through the percolation of shear transformation zones (STZs) along planes of maximum shear stress [37]. This process often triggers a vortex-like mechanism described by MD [38] as well as more mesoscale models [39]. It also leads to structural rejuvenation within the shear band, which subsequently stabilizes the flow [40]. Moreover, MD investigations have demonstrated that the resulting failure mode—brittle localization versus ductile flow—is fundamentally governed by the thermodynamic stability of the glass [41]. In highly stable glasses, yielding occurs as a sharp phase transition with a characteristic stress overshoot, whereas in poorly annealed glasses, it manifests as a smooth crossover to plastic flow [42].

More specifically, for silicate glasses, other MD studies have investigated their mechanical properties with particular focus on the relationship between network topology, plastic flow [43,44], and rupture behavior [45,46]. More recently, significant attention has been devoted to borosilicate glasses [47,48] and their network rearrangement mechanisms. Under tensile loading, it was found that plastic flow promotes the concentration of nonbridging oxygens (NBOs) through

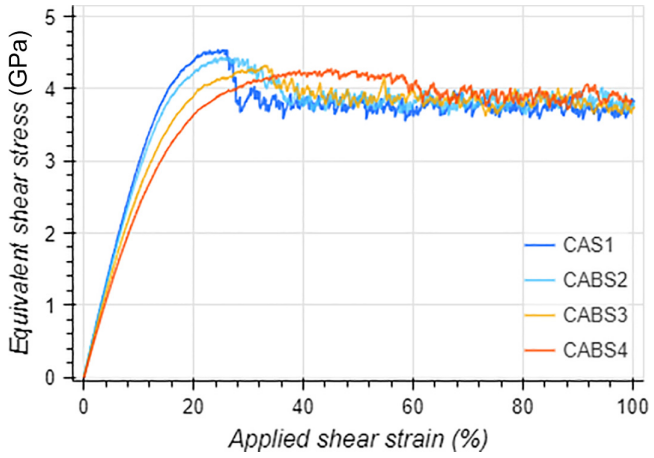

FIG. 6. Stress-strain curves in shear for Ca alumino silicate glasses with increasing boron content.

bond-switching, with fracture initiating preferentially within these NBO-rich, mechanically weakest regions [49,50].

Here, we have employed large-scale molecular dynamics simulations using the SHIK potential [51] to investigate the mechanical behavior of generic borosilicate glasses. More details on the simulation technique can be found in the Supplemental Material [27] Sec. SII. The resulting stress–strain curves under pure shear were calculated as in our previous work [46]. The results are shown in Fig. 6. The addition of boron leaves the flow stress largely unchanged but progressively lowers and broadens the yield-stress peak, thereby reducing the amplitude of strain softening. These combined effects are expected to decrease the susceptibility of the glass to shear banding. Indeed, the localization of mechanical deformation requires a reduction in either strength or stiffness. Compositions exhibiting weaker softening are therefore less prone to shear-band formation, as their shear resistance is only weakly affected by deformation-induced structural transformations. As a result, the shear strength is only marginally influenced, preventing any significant reduction. Shear localization is thus inhibited, leading to more homogeneous deformation, in agreement with the experimental observations.

III. DISCUSSION

There is a longstanding paradox in the fracture behavior of silicate glasses. Classical models of indentation cracking [8,15,52–54] describe fracture in terms of three intrinsic material parameters: elasticity (Young's modulus E), plastic yielding (hardness H), and fracture resistance (toughness K_{IC}). Yet glasses with very similar values of E, H, and K_{IC} can display crack resistances that differ by more than an order of magnitude [9,32,55]. This discrepancy has increasingly directed attention toward a deformation mechanism specific to silicate glasses: irreversible volumetric strain, or densification [14], which accompanies the more conventional volume-conserving shear plastic flow [56,57] during indentation.

Densification is thought to influence crack resistance by modifying the residual stress field generated upon unloading. In this context, the analytic indentation model proposed by Yoffe [15] was indeed able to account for a densification-induced reduction of tensile residual stresses, and thus for a reduction of crack initiation. Because direct measurements of densification remain experimentally challenging [13], it has often been inferred from more accessible proxies, most commonly the recovery of indentation depth at 0.9, T_g (RID) [30]. Several studies have indeed reported strong correlations between crack resistance and RID [4,9,17,32], reinforcing the view that densification plays a central role in glass cracking.

However, this interpretation has recently been questioned. The emphasis placed on densification, and its proxies such as RID or Poisson's ratio, has been challenged [2,55], and Yoffe's model itself has been shown to provide only a crude description of the true indentation stress field [12,13]. These developments suggest that while densification contributes to crack resistance, its role should be more nuanced than previously assumed: additional mechanisms or stress-field complexities must be considered to fully resolve the paradox of glass fracture.

With the present series of glasses, we find no significant correlation between crack resistance and either Poisson's ratio or RID, confirming that neither the composition dependence of elastic properties nor the permanent volumetric deformation modes can be regarded as the primary factors governing crack initiation under indentation. In contrast, by extending earlier approaches [23,33], we observe a broad and robust relationship between crack resistance and the morphology of shear bands in the region where median/radial cracks initiate: glasses exhibiting high crack resistance display homogeneous permanent deformation within the plastic zone.

Note that although plastic flow in silicate glasses is often associated with shear banding, homogeneous irreversible shear deformation has clearly been demonstrated in pillar compression experiments on pure amorphous silica [58]. As composition varies, we observe that shear bands become increasingly pronounced as crack resistance decreases. More precisely, as already noted by Gross *et al.* [23], glasses with greater crack resistance are found to accommodate deformation through a denser network of fine shear bands, implying smaller slip amplitude per band and effectively delaying or preventing the evolution of these bands into critical shear faults.

Because in the present experiments, shear band formation emerges as a key factor affecting crack resistance in silicate glasses, we have leveraged the surface steps left by shear bands at intersecting planes [35] to quantify shear band activity. We have found that indeed the roughness of indent cross sections in crack initiation regions correlates strongly with crack resistance. This relationship provides a quantitative measure of shear localization and is robust across the two glass series studied here, whether strengthened through Mg-for-Ca or B-for-Si substitution. However, this approach has some limitations. The resolution of the laser scanning microscope can not distinguish between glasses with very low roughness due to minimal shear localization. Additionally, fused silica, exhibiting homogeneous plastic shear flow along with densification, is not expected to conform well to this relationship. In this case, minimal roughness is expected while crack resistance measurements are complicated by the prevalence of cone cracks.

This picture is consistent with a broad framework for glassy materials. In many amorphous solids deformed below their glass transition temperature, the dominant mode of plastic deformation is indeed shear bands, which concentrate plastic flow within narrow zones of intense shear strain, whether in glassy polymers [59–61] or in BMG [35,62]. The transition from a stable shear band that accommodates plastic strain to a rapidly propagating crack is triggered by intense localized flow, which may drive severe structural evolution within the band [35,63,64].

Consequently, to reduce shear localization and fracture in bulk metallic glasses, a variety of strategies have been developed. Reducing sample size can induce a brittle to ductile transition by limiting the extent of shear band development [65]. For macroscopic samples, most approaches fall under the general concept of diffusing localization, including the introduction of structural heterogeneity [66], which promotes the nucleation, branching, and intersection of multiple shear bands, the incorporation of nanocrystalline or dendritic inclusions [67], which can nucleate and arrest shear bands but may reduce strength, or even the design of the material for shear induced crystallization in the bands, which adds a strain hardening mechanism [68] thereby mitigating catastrophic localization and enhancing toughness.

The picture is more or less the same for glassy polymers. The morphology of shear bands governs the resulting macroscopic fracture behavior [59]. At high strain rates or low temperatures, deformation typically leads to the formation of individual, coarse 'slip' bands [59,60]. Once these coarse bands extend across the specimen, they serve as brittle failure initiators [61,69]. In contrast, at low strain rates or elevated temperatures, deformation can be accommodated by fine bands organized within broader, diffuse shear zones [59,60,70]. This diffuse mode enables the material to sustain large plastic strains, ultimately producing ductile fracture. As in BMG, a common strengthening mechanism resorts to inclusions with contrasted mechanical properties: soft nanoparticles, for example, can trigger and arrest dilation bands, a specific form of shear bands, with strong enhancement of the fracture toughness [71].

The strong anticorrelation between crack resistance and shear band formation in silicate glasses thus reinforces the broader framework linking plastic flow localization to fracture behavior in silicate glasses. A fully consistent analysis of crack initiation begins at the continuum scale with indentation mechanics. For silicate glasses, this framework may be provided, for example, by Yoffe's model [15], by the more comprehensive formulation of Chiang, Marshall, and Evans (CME) [11], or by more recent finite-element approaches based on constitutive relations [12,55]. From the resulting stress and strain fields, crack-initiation criteria can be postulated and their predictions compared with experimental observations. As an illustration, CME typically invoked a statistical distribution of pre-existing flaws to describe crack initiation: with this approach, a cracking threshold depending solely on the elastic modulus E, the plastic yielding or hardness H, and the fracture toughness K_{IC} emerges. However, CME already recognized that the ultimate origin of median and lateral cracks in glasses most likely lay in flaws associated with discrete shear faults, as documented in the contemporary literature [8,33] and described extensively in the present work. In addition, these early studies emphasized that the major flaws preferentially developed at the intersections of shear faults or flow lines. Notably, analogous mechanisms were reported contemporaneously in other amorphous solids, including the nucleation of cracks at intersecting flow lines in glassy polymers such as polystyrene [59] and poly(methyl methacrylate) [72]. This broader perspective shifts the emphasis from the yield threshold alone to developed shear-flow behavior as a controlling factor in crack initiation, offering a promising route to resolve the glass fracture paradox.

Once posited that resistance to cracking is fundamentally governed by the propensity of the amorphous network to either localize or diffuse shear deformation, the composition dependence can be reconsidered. In "normal" glasses, such as soda-lime silicates, nonbridging oxygens provide pathways of weaker ionic bonding that readily facilitate unstable shear faulting, thereby acting as precursors to extensive crack systems. In contrast, increasing the boron (B_2O_3) content promotes the formation of trigonal boron (III) units and leads to a high density of finer, less damaging shear bands. Importantly, these networks exhibit sizable densification, yet this densification [Fig. 1(c)] does not correlate with crack resistance [Fig. 2(a)], demonstrating that densification is not its primary driver. Instead, it may be a secondary characteristic that sometimes accompanies the structural features enabling shear delocalization. A similar principle applies to the substitution of calcium by magnesium: owing to the high field strength of Mg, the network remains highly connected and largely free of nonbridging oxygens, effectively suppressing the weak links that promote the formation of large, deleterious shear faults [23,26]. The resistance to localization is tightly related to the plastic shear flow properties and the associated structural variations and provides a direct and general basis to the notions of "self-adaptive" [5,25,73] or "flexible and compliant" [1,49] networks.

Unfortunately, despite extensive investigations of metallic glasses and glassy polymers, the relationship between structure, dynamics, and shear-flow localization in amorphous materials remains elusive, limiting a comprehensive understanding of the brittle-to-ductile transition [74]. Beyond the well-known (but as seen here only partial) correlation with Poisson's ratio [75], qualitatively different mechanisms have been suggested, notably through possible connections to the β relaxation [76]. From a modeling standpoint, the transition from sparse plasticity to persistent shear banding, driven for example by the STZ–vortex mechanism [38,77], offers a perspective that may help rationalize the findings of topological constraint approaches and the associated flexible-to-rigid transition [78]. More recently, in generic amorphous systems, a random critical point has been identified that separates these regimes [79], with, for instance, brittle failure governed by the state of the melt relative to the fragile-to-strong transition [80]. However, as these calculations predominantly concern relatively fragile networks in the Angell sense, the present experimental perspective underscores the need for comparable theoretical and modeling efforts focused on more open, covalent networks *i.e.* stronger glasses, before a truly universal theory of the brittle-to-ductile transition in amorphous material is reached.

IV. CONCLUSION

In silicate glasses, the experimentally observed variations in crack resistance far exceed what can be accounted for by changes in elastic, plastic, or fracture-propagation properties alone. Instead, we demonstrate a strong correlation between indentation-induced cracking and shear-band formation across two distinct families of silicate glasses, each exhibiting different toughening mechanisms. This provides compelling evidence that the degree of plastic shear-flow localization is the key controlling factor in crack initiation.

Our findings establish silicate glasses as part of a unified framework alongside bulk metallic glasses and glassy polymers, confirming that shear band formation is a universal determinant of mechanical strength in amorphous solids. From a practical perspective, efforts to mitigate brittleness in silicate glasses should prioritize controlling and diffusing shear localization. Achieving this goal requires deeper insight into the underlying mechanisms and their dependence on glass composition and structure, calling for further intensive research. In this regard, the MD simulations presented in this work demonstrate the strong potential of computational approaches to elucidate these mechanisms and guide future material design.

ACKNOWLEDGMENTS

This work was funded by Agence Nationale de la Recherche, project GaLAaD (Project No. ANR-20-CE08-0002). For open access, the authors have applied a CC-BY public copyright licence to any Author Accepted Manuscript version arising from this submission. We thank Ludovic Olanier and Jean-Claude Mancer for help with the development of the experimental setup.

DATA AVAILABILITY

The data that support the findings of this article are openly available [36].

[1] L. Wondraczek, E. Bouchbinder, A. Ehrlicher, J. C. Mauro, R. Sajzew, and M. M. Smedskjaer, Advancing the mechanical performance of glasses: Perspectives and challenges, Adv. Mater. **34**, 2109029 (2022).

[2] K. Januchta and M. M. Smedskjaer, Indentation deformation in oxide glasses: Quantification, structural changes, and relation to cracking, J. Non-Cryst. Solids: X **1**, 100007 (2019).

[3] L. Wondraczek, J. C. Mauro, J. Eckert, U. Kühn, J. Horbach, J. Deubener, and T. Rouxel, Towards ultrastrong glasses, Adv. Mater. **23**, 4578 (2011).

[4] T. Rouxel, J.-i. Jang, and U. Ramamurty, Indentation of glasses, Prog. Mater. Sci. **121**, 100834 (2021).

[5] K. Januchta, R. E. Youngman, A. Goel, M. Bauchy, S. L. Logunov, S. J. Rzoska, M. Bockowski, L. R. Jensen, and M. M. Smedskjaer, Discovery of ultra-crack-resistant oxide glasses with adaptive networks, Chem. Mater. **29**, 5865 (2017).

[6] D. B. Marshall, R. F. Cook, N. P. Padture, M. L. Oyen, A. Pajares, J. E. Bradby, I. E. Reimanis, R. Tandon, T. F. Page, G. M. Pharr, *et al.*, The compelling case for indentation as a functional exploratory and characterization tool, J. Am. Ceram. Soc. **98**, 2671 (2015).

[7] M. Wada, H. Furukawa, and K. Fujita, Crack resistance of glass on Vickers indentation, *Proceedings of the Tenth International Congress on Glass* (Ceramic Society of Japan, Tokyo, 1974), Vol. 11, pp. 39–46.

[8] B. R. Lawn, A. G. Evans, and D. B. Marshall, Elastic/plastic indentation damage in ceramics: The median/radial crack system, J. Am. Ceram. Soc. **63**, 574 (1980).

[9] Y. Kato, H. Yamazaki, S. Yoshida, and J. Matsuoka, Effect of densification on crack initiation under Vickers indentation test, J. Non-Cryst. Solids **356**, 1768 (2010).

[10] B. R. Lawn and E. R. Fuller, Equilibrium penny-like cracks in indentation fracture, J. Mater. Sci. **10**, 2016 (1975).

[11] S. Chiang, D. Marshall, and A. Evans, The response of solids to elastic/plastic indentation. i. stresses and residual stresses, J. Appl. Phys. **53**, 298 (1982).

[12] B. C. Davis, G. S. Glaesemann, and I. Reimanis, Sharp indentation stress fields in fused silica: Finite element analysis and Yoffe analytic model, J. Am. Ceram. Soc. **103**, 7135 (2020).

[13] G. A. Rosales-Sosa, E. Barthel, Y. Kato, M. Bourguignon, A. Yamada, T. Inoue, S. Nakane, and H. Yamazaki, Indentation stress fields in brittle materials: A micro-photoelastic investigation in silicate glasses, Acta Mater. **292**, 120973 (2025).

[14] F. M. Ernsberger, Role of densification in deformation of glasses under point loading, J. Am. Ceram. Soc. **51**, 545 (1968).

[15] E. Yoffe, Elastic stress fields caused by indenting brittle materials, Philos. Mag. A **46**, 617 (1982).

[16] L. M. Cook, Chemical processes in glass polishing, J. Non-Cryst. Solids **120**, 152 (1990).

[17] T. Rouxel, Driving force for indentation cracking in glass: composition, pressure and temperature dependence, Philos. Trans. R. Soc. A **373**, 20140140 (2015).

[18] M. Barlet, J.-M. Delaye, T. Charpentier, M. Gennisson, D. Bonamy, T. Rouxel, and C. L. Rountree, Hardness and toughness of sodium borosilicate glasses via Vickers's indentations, J. Non-Cryst. Solids **417-418**, 66 (2015).

[19] S. Yoshida, Compositional variation of indentation-induced deformation and cracking in glass, J. Ceram. Soc. Jpn. **128**, 340 (2020).

[20] J. Hagan, Micromechanics of crack nucleation during indentations, J. Mater. Sci. **14**, 2975 (1979).

[21] B. R. Lawn, T. P. Dabbs, and C. J. Fairbanks, Kinetics of shear-activated indentation crack initiation in soda-lime glass, J. Mater. Sci. **18**, 2785 (1983).

[22] S. Lathabai, J. Rödel, T. Dabbs, and B. R. Lawn, Fracture mechanics model for subthreshold indentation flaws: Part I equilibrium fracture, J. Mater. Sci. **26**, 2157 (1991).

[23] T. Gross, J. Wu, D. Baker, J. Price, and R. Yongsunthon, Crack-resistant glass with high shear band density, J. Non-Cryst. Solids **494**, 13 (2018).

[24] Y. Kato, H. Yamazaki, Y. Kubo, S. Yoshida, J. Matsuoka, and T. Akai, Effect of B_2O_3 content on crack initiation under Vickers indentation test, J. Ceram. Soc. Jpn. **118**, 792 (2010).

[25] K. Osada, A. Yamada, T. Ohuchi, S. Yoshida, and J. Matsuoka, Transition in deformation mechanism of aluminosilicate glass at high pressure and room temperature, J. Am. Ceram. Soc. **103**, 6755 (2020).

[26] A. L. Fry, A. L. Ogrinc, S. H. Kim, and J. C. Mauro, Field strength effect on elastoplastic behavior of aluminoborosilicate glass: II. Volumetric recovery, J. Am. Ceram. Soc. **106**, 5213 (2023).

[27] See Supplemental Material at http://link.aps.org/supplemental/10.1103/l936-nk13 for more details on the experimental procedures and the numerical calculations, which also includes Refs. [9,23,33,51,56,81–85].

[28] Y. H. F. Gomes, G. A. Rosales-Sosa, S. Nakane, Y. Kato, H. Yamazaki, A. Yamada, and H. Eckert, Structural changes upon ambient temperature densification in calcium aluminoborosilicate glasses: Relation to indentation crack resistance, J. Phys. Chem. C **129**, 18772 (2025).

[29] Y. Kato, H. Yamazaki, S. Itakura, S. Yoshida, and J. Matsuoka, Load dependence of densification in glass during Vickers indentation test, J. Ceram. Soc. Jpn. **119**, 110 (2011).

[30] S. Yoshida, J.-C. Sangleboeuf, and T. Rouxel, Quantitative evaluation of indentation-induced densification in glass, J. Mater. Res. **20**, 3404 (2005).

[31] T. Rouxel, H. Ji, T. Hammouda, and A. Moreac, Poisson's ratio and the densification of glass under high pressure, Phys. Rev. Lett. **100**, 225501 (2008).

[32] P. Sellappan, T. Rouxel, F. Celarie, E. Becker, P. Houizot, and R. Conradt, Composition dependence of indentation deformation and indentation cracking in glass, Acta Mater. **61**, 5949 (2013).

[33] J. T. Hagan, Shear deformation under pyramidal indentations in soda-lime glass, J. Mater. Sci. **15**, 1417 (1980).

[34] K.-W. Chen and J.-F. Lin, Investigation of the relationship between primary and secondary shear bands induced by indentation in bulk metallic glasses, Int. J. Plast. **26**, 1645 (2010).

[35] C. Schuh, T. Hufnagel, and U. Ramamurty, Mechanical behavior of amorphous alloys, Acta Mater. **55**, 4067 (2007).

[36] M. Bourguignon, G. A. Rosales-Sosa, and Y. Kato, Crack resistance and roughness data, Zenodo (2026), doi:10.5281/zenodo.19224392.

[37] Y. Shi and M. L. Falk, Strain localization and percolation of stable structure in amorphous solids, Phys. Rev. Lett. **95**, 095502 (2005).

[38] D. Şopu, A. Stukowski, M. Stoica, and S. Scudino, Atomic-level processes of shear band nucleation in metallic glasses, Phys. Rev. Lett. **119**, 195503 (2017).

[39] V. Hieronymus-Schmidt, H. Rösner, G. Wilde, and A. Zaccone, Shear banding in metallic glasses described by alignments of Eshelby quadrupoles, Phys. Rev. B **95**, 134111 (2017).

[40] A. Barbot, M. Lerbinger, A. Lemaître, D. Vandembroucq, and S. Patinet, Rejuvenation and shear banding in model amorphous solids, Phys. Rev. E **101**, 033001 (2020).

[41] D. Richard, M. Ozawa, S. Patinet, E. Stanifer, B. Shang, S. A. Ridout, B. Xu, G. Zhang, P. K. Morse, J.-L. Barrat, L. Berthier, M. L. Falk, P. Guan, A. J. Liu, K. Martens, S. Sastry, D. Vandembroucq, E. Lerner, and M. L. Manning, Predicting plasticity in disordered solids from structural indicators, Phys. Rev. Mater. **4**, 113609 (2020).

[42] M. Ozawa, L. Berthier, G. Biroli, A. Rosso, and G. Tarjus, Random critical point separates brittle and ductile yielding transitions in amorphous materials, Proc. Natl. Acad. Sci. USA **115**, 6656 (2018).

[43] B. Mantisi, G. Kermouche, E. Barthel, and A. Tanguy, Impact of pressure on plastic yield in amorphous solids with open structure, Phys. Rev. E **93**, 033001 (2016).

[44] G. Molnár, P. Ganster, A. Tanguy, E. Barthel, and G. Kermouche, Densification dependent yield criteria for sodium silicate glasses–an atomistic simulation approach, Acta Mater. **111**, 129 (2016).

[45] F. Yuan and L. Huang, Brittle to ductile transition in densified silica glass, Sci. Rep. **4**, 5035 (2014).

[46] G. Molnár, P. Ganster, and A. Tanguy, Effect of composition and pressure on the shear strength of sodium silicate glasses: An atomic scale simulation study, Phys. Rev. E **95**, 043001 (2017).

[47] L. Deng and J. Du, Development of boron oxide potentials for computer simulations of multicomponent oxide glasses, J. Am. Ceram. Soc. **102**, 2482 (2019).

[48] H. Liu, B. Deng, S. Sundararaman, Y. Shi, and L. Huang, Understanding the response of aluminosilicate and aluminoborate glasses to sharp contact loading using molecular dynamics simulation, J. Appl. Phys. **128**, 035106 (2020).

[49] K. Lee, Y. Yang, L. Ding, B. Ziebarth, M. J. Davis, and J. C. Mauro, Plasticity of borosilicate glasses under uniaxial tension, J. Am. Ceram. Soc. **103**, 4295 (2020).

[50] K. Lee, Y. Yang, L. Ding, B. Ziebarth, M. J. Davis, and J. C. Mauro, Pressure effects on shear deformation of borosilicate glasses, J. Am. Ceram. Soc. **104**, 3073 (2021).

[51] Y.-T. Shih, S. Sundararaman, S. Ispas, and L. Huang, New interaction potentials for alkaline earth silicate and borate glasses, J. Non-Cryst. Solids **565**, 120853 (2021).

[52] B. Lawn and A. Evans, A model for crack initiation in elastic/plastic indentation fields, J. Mater. Sci. **12**, 2195 (1977).

[53] S. S. Chiang, D. B. Marshall, and A. G. Evans, The response of solids to elastic/plastic indentation. ii. fracture initiation, J. Appl. Phys. **53**, 312 (1982).

[54] G. Feng, S. Qu, Y. Huang, and W. Nix, An analytical expression for the stress field around an elastoplastic indentation/contact, Acta Mater. **55**, 2929 (2007).

[55] E. Barthel, V. Keryvin, G. Rosales-Sosa, and G. Kermouche, Indentation cracking in silicate glasses is directed by shear flow, not by densification, Acta Mater. **194**, 473 (2020).

[56] K. Peter, Densification and flow phenomena of glass in indentation experiments, J. Non-Cryst. Solids **5**, 103 (1970).

[57] A. Arora, D. Marshall, B. Lawn, and M. Swain, Indentation deformation/fracture of normal and anomalous glasses, J. Non-Cryst. Solids **31**, 415 (1979).

[58] G. Kermouche, G. Guillonneau, J. Michler, J. Teisseire, and E. Barthel, Perfectly plastic flow in silica glass, Acta Mater. **114**, 146 (2016).

[59] J. B. C. Wu and J. C. M. Li, Slip processes in the deformation of polystyrene, J. Mater. Sci. **11**, 434 (1976).

[60] C. B. Bucknall, *Toughened Plastics* (Applied Science Publishers, Springer, Dordrecht, 1977).

[61] A. S.Argon, *The Physics of Deformation and Fracture of Polymers* (Cambridge University Press, Cambridge, 2013).

[62] A. Argon, Plastic deformation in metallic glasses, Acta Metall. **27**, 47 (1979).

[63] J. Li, F. Spaepen, and T. C. Hufnagel, Nanometre-scale defects in shear bands in a metallic glass, Philos. Mag. A **82**, 2623 (2002).

[64] A. Nicolas, E. E. Ferrero, K. Martens, and J.-L. Barrat, Deformation and flow of amorphous solids: An updated review of mesoscale elastoplastic models, Rev. Mod. Phys. **90**, 045006 (2018).

[65] D. Tönnies, R. Maaß, and C. A. Volkert, Room temperature homogeneous ductility of micrometer-sized metallic glass, Adv. Mater. **26**, 5715 (2014).

[66] J. Das, M. B. Tang, K. B. Kim, R. Theissmann, F. Baier, W. H. Wang, and J. Eckert, "Work-hardenable" ductile bulk metallic glass, Phys. Rev. Lett. **94**, 205501 (2005).

[67] D. C. Hofmann, J.-Y. Suh, A. Wiest, G. Duan, M.-L. Lind, M. D. Demetriou, and W. L. Johnson, Designing metallic glass matrix composites with high toughness and tensile ductility, Nature (London) **451**, 1085 (2008).

[68] M. Chen, A. Inoue, W. Zhang, and T. Sakurai, Extraordinary plasticity of ductile bulk metallic glasses, Phys. Rev. Lett. **96**, 245502 (2006).

[69] K. Friedrich, Crazes and shear bands in semi-crystalline thermoplastics, in *Crazing in Polymers*, edited by H. H. Kausch (Springer Berlin Heidelberg, Berlin, Heidelberg, 1983), pp. 225–274.

[70] P. B. Bowden and S. Raha, The formation of micro shear bands in polystyrene and polymethylmethacrylate, Philos. Mag. **22**, 463 (1970).

[71] A. Lazzeri and C. Bucknall, Applications of a dilatational yielding model to rubber-toughened polymers, Polymer **36**, 2895 (1995).

[72] J. Ritter, M. Lin, and T. Lardner, Strength of poly(methyl methacrylate) with indentation flaws, J. Mater. Sci. **23**, 2370 (1988).

[73] X. Ke, Z. Shan, Z. Li, Y. Tao, Y. Yue, and H. Tao, Toward hard and highly crack-resistant magnesium aluminosilicate glasses and transparent glass-ceramics, J. Am. Ceram. Soc. **103**, 3600 (2020).

[74] A. Tanguy, Elasto-plastic behavior of amorphous materials: a brief review, Comptes Rendus. Physique **22**, 117 (2021).

[75] J. J. Lewandowski, W. H. Wang, and A. L. Greer, Intrinsic plasticity or brittleness of metallic glasses, Philos. Mag. Lett. **85**, 77 (2005).

[76] J. Qiao and J. Pelletier, Dynamic mechanical relaxation in bulk metallic glasses: A review, J. Mater. Sci. Technol. **30**, 523 (2014).

[77] H. Rösner, A. Bera, and A. Zaccone, Unveiling the asymmetry in density within the shear bands of metallic glasses, Phys. Rev. B **110**, 014107 (2024).

[78] M. Bauchy, B. Wang, M. Wang, Y. Yu, M. J. Abdolhosseini Qomi, M. M. Smedskjaer, C. Bichara, F.-J. Ulm, and R. Pellenq, Fracture toughness anomalies: Viewpoint of topological constraint theory, Acta Mater. **121**, 234 (2016).

[79] L. Berthier, G. Biroli, L. Manning, and F. Zamponi, Yielding and plasticity in amorphous solids, Nat. Rev. Phys. **7**, 313 (2025).

[80] A. Atila, S. V. Sukhomlinov, M. J. Honecker, and M. H. Müser, Plasticity of metallic glasses dictated by their state at the fragile-to-strong transition temperature, Acta Mater. **286**, 120753 (2025).

[81] S. Sundararaman, L. Huang, S. Ispas, and W. Kob, New optimization scheme to obtain interaction potentials for oxide glasses, J. Chem. Phys. **148**, 194504 (2018).

[82] D. Wolf, P. Keblinski, S. R. Phillpot, and J. Eggebrecht, Exact method for the simulation of Coulombic systems by spherically truncated, pairwise r^{-1} summation, J. Chem. Phys. **110**, 8254 (1999).

[83] R. Buckingham, The classical equation of state of gaseous helium, neon, and argon, Proc. R. Soc. London A **168**, 264 (1938).

[84] G. Molnár, P. Ganster, J. Török, and A. Tanguy, Sodium effect on static mechanical behavior of MD-modeled sodium silicate glasses, J. Non-Cryst. Solids **440**, 12 (2016).

[85] A. Makishima and J. Mackenzie, Direct calculation of Young's modulus of glass, J. Non-Cryst. Solids **12**, 35 (1973).